Cell Metabolism
Short Article

Autophagy Is Required to Maintain Muscle Mass

Eva Masiero,[1,2,4] Lisa Agatea,[2] Cristina Mammucari,[4] Bert Blaauw,[2,3] Emanuele Loro,[2] Masaaki Komatsu,[5] Daniel Metzger,[6] Carlo Reggiani,[3] Stefano Schiaffino,[2,4] and Marco Sandri[1,2,4,*]
[1]Dulbecco Telethon Institute, via Orus 2, 35129 Padova, Italy
[2]Venetian Institute of Molecular Medicine, via Orus 2, 35129 Padova, Italy
[3]Department of Human Anatomy and Physiology
[4]Department of Biomedical Science
University of Padova, viale Colombo 3, Padova, Italy
[5]Tokyo Metropolitan Institute of Medical Science, Tokyo, Japan
[6]Centre National de la Recherche Scientifique, INSERM, Illkirch-Cedex, France
*Correspondence: marco.sandri@unipd.it
DOI 10.1016/j.cmet.2009.10.008

SUMMARY

The ubiquitin-proteasome and autophagy-lysosome pathways are the two major routes for protein and organelle clearance. In skeletal muscle, both systems are under FoxO regulation and their excessive activation induces severe muscle loss. Although altered autophagy has been observed in various myopathies, the specific role of autophagy in skeletal muscle has not been determined by loss-of-function approaches. Here, we report that muscle-specific deletion of a crucial autophagy gene, *Atg7*, resulted in profound muscle atrophy and age-dependent decrease in force. *Atg7* null muscles showed accumulation of abnormal mitochondria, sarcoplasmic reticulum distension, disorganization of sarcomere, and formation of aberrant concentric membranous structures. Autophagy inhibition exacerbated muscle loss during denervation and fasting. Thus, autophagy flux is important to preserve muscle mass and to maintain myofiber integrity. Our results suggest that inhibition/alteration of autophagy can contribute to myofiber degeneration and weakness in muscle disorders characterized by accumulation of abnormal mitochondria and inclusions.

INTRODUCTION

Macroautophagy, hereafter referred to as autophagy, is a highly conserved homeostatic process carrying out degradation of cytoplasmic components including damaged organelles, toxic protein aggregates and intracellular pathogens (Mizushima et al., 2008). Autophagy takes place at basal levels in all eukaryotic cells, turning over long-lived macromolecules and large supramolecular structures including whole organelles to rejuvenate their function. In addition, autophagy can be upregulated during metabolic, genotoxic, or hypoxic stress conditions and acts as an adaptive mechanism essential for cell survival. Skeletal muscle is a major site of metabolic activity—and the most abundant tissue in the human body, accounting for about 40% of the total body mass. Being the largest protein reservoir, muscle serves as a source of amino acids to be utilized for energy production by various organs during catabolic periods (Lecker et al., 2006). For instance, amino acids generated from muscle protein breakdown are utilized by the liver to produce glucose and to support acute phase protein synthesis (Lecker et al., 2006). Protein degradation in skeletal muscle, like in all the mammalian cells, is controlled by the two major proteolytic systems, the ubiquitin proteasome and the autophagy lysosome. Both degradation pathways are activated in a number of catabolic disease states, including cancer, AIDS, diabetes, and heart and renal failure and contribute to muscle loss and weakness. The two systems are controlled by a transcriptional program that upregulates few critical and rate-limiting enzymes (Sandri, 2008). We have recently identified FoxO transcription factors as the main coordinators of the two proteolytic pathways by inducing several autophagy-related genes as well as the two muscle-specific ubiquitin ligases *atrogin-1* and *MuRF1* (Mammucari et al., 2007; Sandri et al., 2004). While ubiquitin-preoteasome dependent degradation has been deeply investigated and its contribution to muscle loss has been already well documented, the role of autophagy in regulating muscle mass has just started to be studied. Excessive activation of autophagy aggravates muscle wasting (Dobrowolny et al., 2008; Mammucari et al., 2007; Wang et al., 2005; Zhao et al., 2007) by removing portion of cytoplasm, proteins, and organelles. Conversely, inhibition of lysosome-dependent degradation causes myopathies like Pompe and Danon diseases, and autophagy inhibition is thought to play a role in many myopathies with inclusions or with abnormal mitochondria (Levine and Kroemer, 2008; Temiz et al., 2009). However, the exact role of autophagy in physiology of skeletal muscle has never been addressed. Thus, defining the role of autophagy in skeletal muscle homeostasis is critical for understanding the pathogenesis of different diseases and for developing new therapies against muscle loss. To clarify this issue we have generated conditional knockout for *Atg7* gene to block autophagy specifically in skeletal muscle.

RESULTS

Generation of Muscle-Specific Atg7 Knockout Mice

We crossed *Atg7*-floxed mice ($Atg7^{f/f}$) with a transgenic line expressing Cre recombinase under the control of a myosin light chain 1 fast promoter to generate muscle-specific *Atg7*-knockout mice, which are hereafter referred to as $Atg7^{-/-}$. PCR analysis

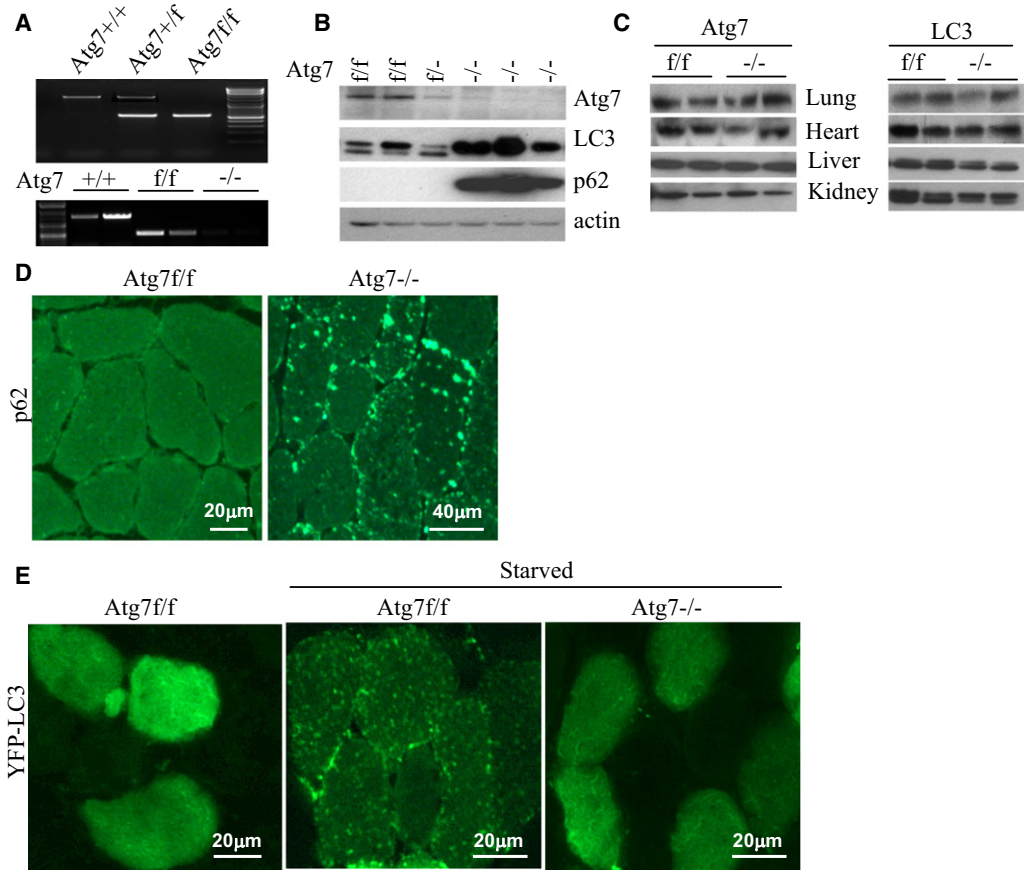

Figure 1. Generation of Muscle-Specific Atg7-Knockout (Atg7$^{-/-}$) Mice

(A) Upper panel, genotyping of the *Atg7$^{f/f}$* mice. Lower panel, PCR analysis with genomic DNA from gastrocnemius muscle. One of the two PCR primers is inside the floxed region. Absence of a PCR product revealed an efficient Cre-mediated recombination of lox-P sites.

(B) Impaired LC3 lipidation and accumulation of p62 protein in Atg7$^{-/-}$ muscles. Muscle homogenates were immunoblotted with antibodies against Atg7, LC3, and p62.

(C) Immunoblot analysis of Atg7 and LC3 in homogenates from different tissues.

(D) Immunohistochemistry for p62 showed aggregates in Atg7$^{-/-}$ muscles but not in Atg7$^{f/f}$ mice.

(E) Autophagosome formation induced by fasting is suppressed in Atg7$^{-/-}$ mice. Muscles of Atg7$^{f/f}$ and Atg7$^{-/-}$ were transfected by electroporation with plasmid coding for YFP-LC3. Eight days later, mice were fasted for 24 hr before sacrifice. Myofibers expressing YFP-LC3 were analyzed by fluorescent microscopy.

confirmed deletion of floxed sequence in genomic DNA from skeletal muscle (Figure 1A). Accordingly, Atg7 protein was almost undetectable in muscles of homozygous mice and considerably reduced in heterozygous animals (Figure 1B). Traces of persistent Atg7 protein are due to endothelial cells, fibroblasts, macrophages, and blood cells. Efficient inhibition of autophagy in skeletal muscles was confirmed by suppression of LC3 lipidation and accumulation of p62 and LC3 proteins in extracts of adult fast and slow muscles (Figures 1B and S1A). LC3 exists in two forms: the free mature form (LC3I) and the faster lipidated LC3 (LC3II). The absence of LC3II band confirms that the reaction of LC3 conjugation to phospholipids was completely blocked. LC3 and p62 proteins are known to be sequestered into the autophagosomes and lost when autophagosomes fuse with lysosomes. Thus, their increase indicates an efficient inhibition of autophagy. Conversely, Atg7 protein was detected and LC3I to LC3II conversion was unaffected in other tissues including heart (Figure 1C). Moreover, immunohistochemical analyses showed the presence of p62 aggregates in myofibers of Atg 7$^{-/-}$ mice (Figure 1D). To further confirm that autophagic vesicles formation was blocked, we transfected adult skeletal muscle with YFP-LC3, and 1 week later we starved the mice (Mammucari et al., 2007). Ablation of *Atg7* in fasted muscle completely abolished the formation of YFP-LC3 positive autophagosomes in myofibers (Figure 1E). Altogether, these findings validate our genetic mouse model of muscle-specific inhibition of the autophagy system.

Autophagy Inhibition Induces Muscle Atrophy, Loss-of-Force Production, and Morphological Features of Myopathy

The resulting Atg7$^{-/-}$ mice were indistinguishable in appearance from age-matched control Atg7$^{+/+}$ mice. However, the growth curve showed a slight reduction of body growth, which started to differ from control after about 40 days from birth (Figure S2). Morphological analysis of adult muscles revealed degenerative changes, including vacuolated and centrally nucleated myofiber, and a general decrease in myofiber size at 2 months of age (Figures 2A and 2B). A few fibers were positive for immunoglobulin

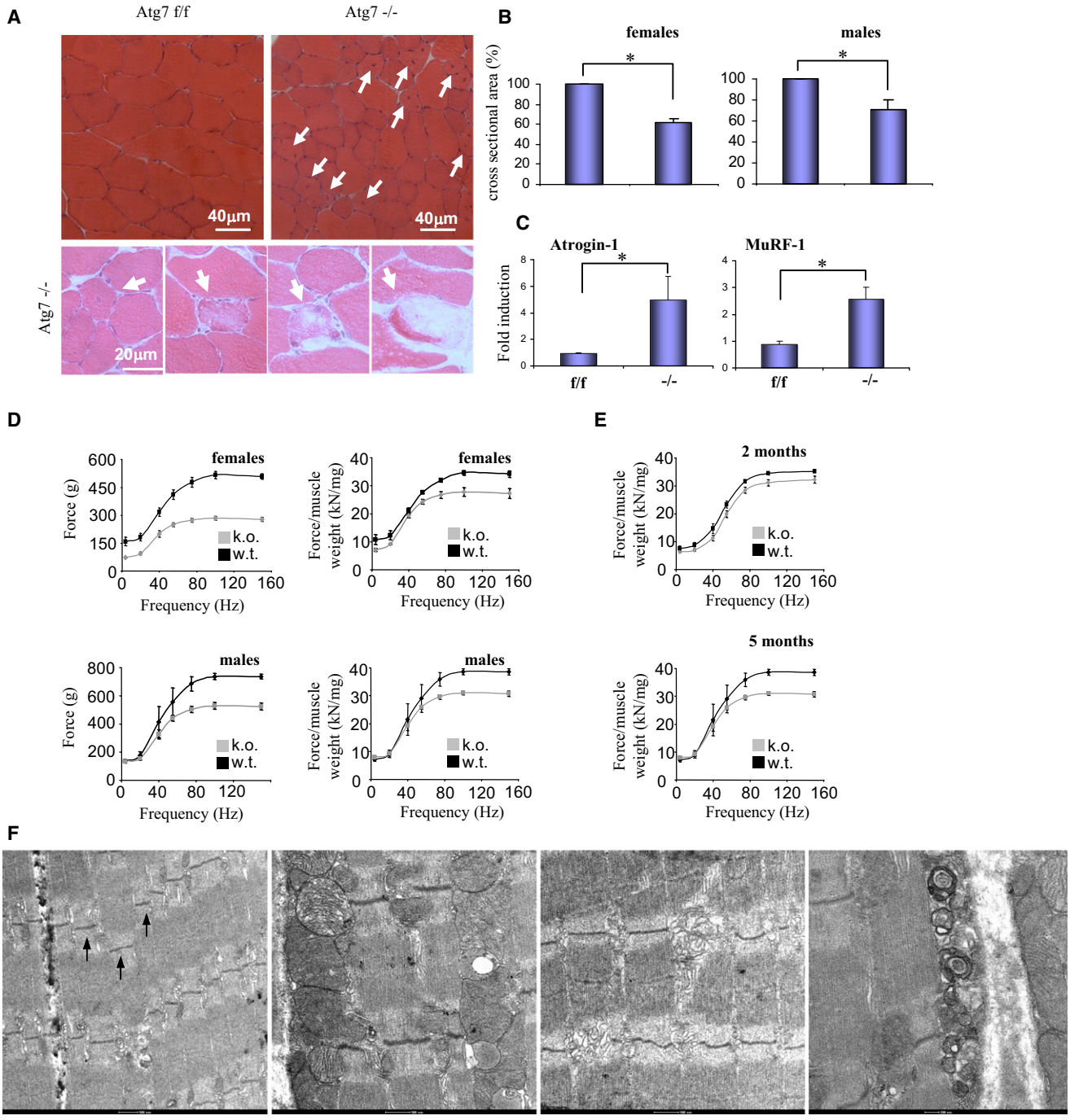

Figure 2. Morphological and Functional Changes in Muscles of Atg7$^{-/-}$ Mice Reveal Muscle Dysfunction and Features of Myopathy

(A) H&E staining showing a general decrease in myofibers size and different features of muscle degeneration (white arrows), including central nuclei and vacuolated fibers.

(B) Quantification of cross-sectional area (CSA) of myofibers. Values are mean ± SEM of data from five mice in each group.

(C) Upregulation of the critical atrophy-related and muscle specific genes in adult skeletal muscle of Atg7$^{-/-}$. RNA was extracted from TA muscles, and quantitative PCR analysis was performed in triplicates using specific oligonucleotides (see Table S1). Data were normalized to the β-actin content and expressed as fold increase over levels of Atg7$^{f/f}$ muscles, data are mean ± SEM. (*$p < 0.001$).

(D) Force measurements performed in vivo showed that Atg7$^{-/-}$ led to a profound decrease in force generation especially of maximal force generated during tetanic contraction. The force is still significantly reduced even when the absolute tetanic force is normalized for the muscle weight (n = 5); data are mean ± SEM.

(E) Age aggravated the impairment of force production.

(F) Electron micrographs of Atg7$^{-/-}$ EDL muscles.

staining as a consequence of membrane permeabilization, suggesting the presence of rare necrotic events, which, however do not modify creatine kinase blood levels. Myosin composition was not affected in Atg7$^{-/-}$ muscles (Figures S3 and S4). The frequency of centrally nucleated fibers slowly increased with age (Figure S5A). Importantly myofiber degeneration is not caused by alteration in dystrophin expression and localization (Figure S6). Quantification of cross-sectional area showed a 40% decrease in myofiber size both in females and males (Figures 2B and S7). Further characterization displayed no difference between fiber types; both glycolitic and oxidative fibers undergo muscle atrophy (Figure S8). The muscle-to-body weight ratio was also decreased, suggesting an important waste of muscle tissue (Figure S9). Loss of muscle mass is controlled by a transcriptional program that requires activation of a subset of genes named atrophy-related genes or atrogenes (Lecker et al., 2004). Thus, we monitored the level of expression of atrogenes involved in the ubiquitin proteasome. Indeed, the two atrophy-related ubiquitin ligases *atrogin-1* and *MuRF1*, as well as genes involved in different catabolic pathways, were upregulated in Atg7$^{-/-}$ muscles at basal state (Figures 2C and S10). The upregulation of the ubiquitin ligases is associated with FoxO1 dephosphorylation and activation (Figure S11). Interestingly, proteasomal function is not impaired in Atg7 null muscles but instead is increased (Figure S12). Inhibition of autophagy led also to induction of apoptosis (Figure S12). Altogether, these results suggest that deletion of Atg7 triggers compensatory upregulation of ubiquitin proteasome system and activation of apoptosis, which contribute, at least partially, to muscle loss.

Next, we asked whether muscle atrophy is accompanied by changes of muscle force in living animals. Physiological analyses showed a marked reduction in absolute force independently of gender (Figure 2D). Importantly, when the absolute force was normalized for the muscle mass, the resulting specific force was still significantly decreased. Thus, not only do the muscles become smaller but there is a general impairment in force transmission that leads to profound weakness. Importantly, force drop was age dependent since 5-month-old males showed a more important decrease in specific force, when compared to age-matched control littermates, than 2-month-old mice (Figure 2E). To understand the important impairment in force generation, we performed electron-microscopy studies. Several changes were detected in Atg7$^{-/-}$ muscles including misalignment of Z-line, accumulation of big abnormal mitochondria which in some cases span from one to the next Z line, presence of swollen mitochondria, sarcoplasmic reticulum distension, and formation of aberrant concentric membranous structure (Figures 2F and S13) similar to those observed in Atg7-deficient livers and Atg5-deficient hearts (Komatsu et al., 2005; Nakai et al., 2007). The alteration of mitochondrial morphology is associated with oxidative stress, as revealed by increased protein carbonylation and expression of antioxidant genes, but apparently not to energy unbalance, since AMPK was not activated (Figures S14A–S14C). In addition, the changes of sarcoplasmic reticulum are related with a markedly increased phosphorylation, and therefore inhibition, of the translation initiation factor eIF2α, which is known to lead to suppression of ribosome assembly and protein synthesis. Altogether, the phosphorylation of eIF2α and the increase of the endoplasmic reticulum (ER) chaperone, BiP/GRP78, are consistent with an unfolding protein response (Figure S15).

Inhibition of Autophagy Exacerbates Muscle Loss and Degeneration in Catabolic Conditions

Next, we wanted to clarify the contribution and the role of autophagy under conditions of muscle wasting. We used two models of muscle atrophy, fasting and denervation, and we compared Atg7 null muscles with controls. Inhibition of autophagy did not prevent muscle loss and activation of the atrophy-related program in denervated muscles. On the contrary, autophagy-deficient animals lost significantly more muscle mass than control ones (Figure 3A). Expression of several atrophy-related genes, including *MuRF1*, *cathepsin L*, and *Bnip3l*, were more upregulated in atrophying muscles of Atg7$^{-/-}$ muscles, which suggest a more important activation of the atrophy program (Figures 3B and S16). Morphological observations showed different features of myopathy in denervated Atg7$^{-/-}$ muscles, including presence of abnormal myonuclei, accumulation of hematoxylin-positive inclusions, and vacuolated area, which were present only in autophagy-deficient muscles (Figures 3C and S17). Electron microscopy revealed the presence of concentric membranous structures embedded into an electron-opaque amorphous material (Figure 3D). Interestingly, p62 aggregates were increased in size and number in denervated myofibers of Atg7$^{-/-}$ mice compared to innervated muscles (Figure 3E). The p62-positive aggregates were also positive for ubiquitin (Figures 3F and S18). Accordingly, p62 and ubiquitinated proteins greatly accumulate in detergent soluble and insoluble fractions of autophagy-deficient denervated muscles (Figures 3G and S19). Thus, autophagy inhibition does not preserve muscle mass during catabolic conditions and, surprisingly, exacerbates muscle loss during denervation.

We next examined muscle atrophy induced by fasting. Atg7$^{-/-}$ and Atg7$^{+/+}$ muscles showed similar upregulation of atrophy-related genes, which reflects no major difference in the changes of Akt phosphorylation and downstream targets (Figures 4A and 4B). However, the morphological features of muscle degeneration were more evident. Many small flattened or irregularly shaped fibers containing hematoxylin-positive inclusions as well as fibers with fragmented and vacuolated cytosol appeared in Atg7$^{-/-}$ muscles during fasting (Figure 4C). Electron microscopy revealed an increase of the concentric membranous structures (Figure 4D). However, fasted muscles never showed the amorphous material detected in denervated muscles. Interestingly, p62 aggregates were similar or smaller than the ones found in fed Atg7$^{-/-}$ muscles and certainly never reached the size of those observed in denervated muscles (Figure 4E). Indeed, p62 did not accumulate in detergent-soluble and -insoluble fractions of starved muscles (Figure S20). Thus, autophagy plays different roles and importance in different conditions of muscle loss but seems to be always crucial for maintaining normal homeostasis of muscle mass in physiological and pathological conditions.

Deletion of *Atg7* Gene in Adulthood Triggers Muscle Loss and Weakness

To further check the role of autophagy in adulthood, we generated tamoxifen-inducible muscle-specific Atg7 knockout mice.

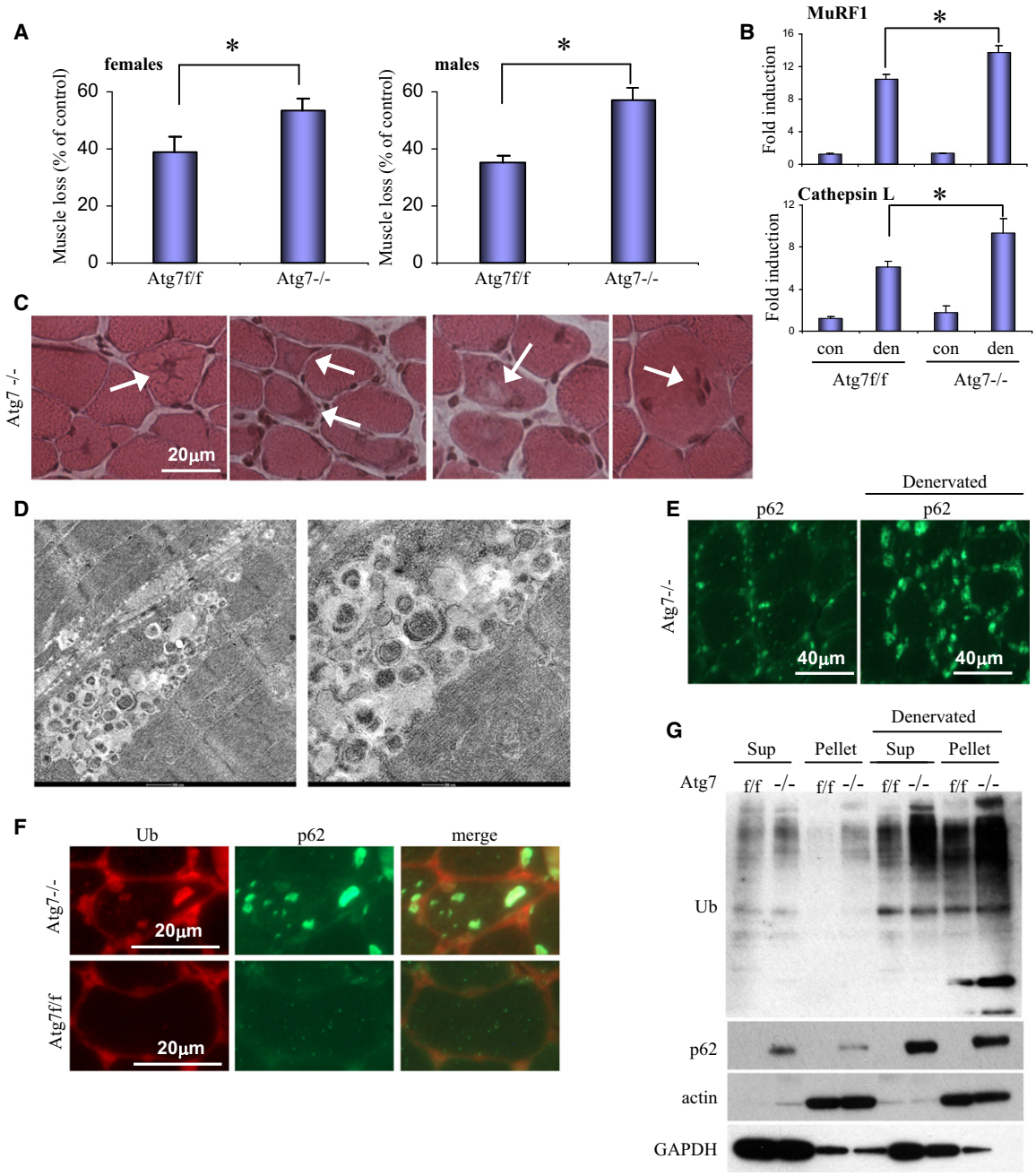

Figure 3. Denervation Aggravates Morphological Abnormalities and Muscle Loss in Atg7$^{-/-}$ Muscles

(A) Quantification of muscle loss after 2 weeks from denervation. CSA of innervated and denervated fibers was measured. Muscle loss is expressed as percentage of decrease of cross-sectional areas of denervated fibers versus innervated ones. More than 1000 fibers per each muscle were counted (n = 4); data are mean ± SEM (*p < 0.001).

(B) Enhanced upregulation of the atrophy-related genes in denervated skeletal muscles of Atg7$^{-/-}$ mice. Data are mean ± SEM (*p < 0.01).

(C) H&E staining showing accumulation of hematoxylin-positive structures, vacuolated areas, and abnormal nuclei (white arrows) in denervated Atg7$^{-/-}$.

(D) Electron micrographs of denervated Atg7$^{-/-}$ showing aberrant concentric membranous structures dispersed between amorphous electron opaque material.

(E) Immunostaining for anti-p62 showed that p62 aggregates increased in size and number in denervated muscle of Atg7$^{-/-}$.

(F) Double imunofluorescence staining reveals the colocalization of p62 and ubiquitin.

(G) Increase of ubiquitinated proteins and of p62 in Atg7$^{-/-}$ muscles during denervation. Detergent-soluble (Sup) and -insoluble (Pellet) fractions of control and denervated muscles were immunoblotted against ubiquitin and p62. Data are representative of three different experiments.

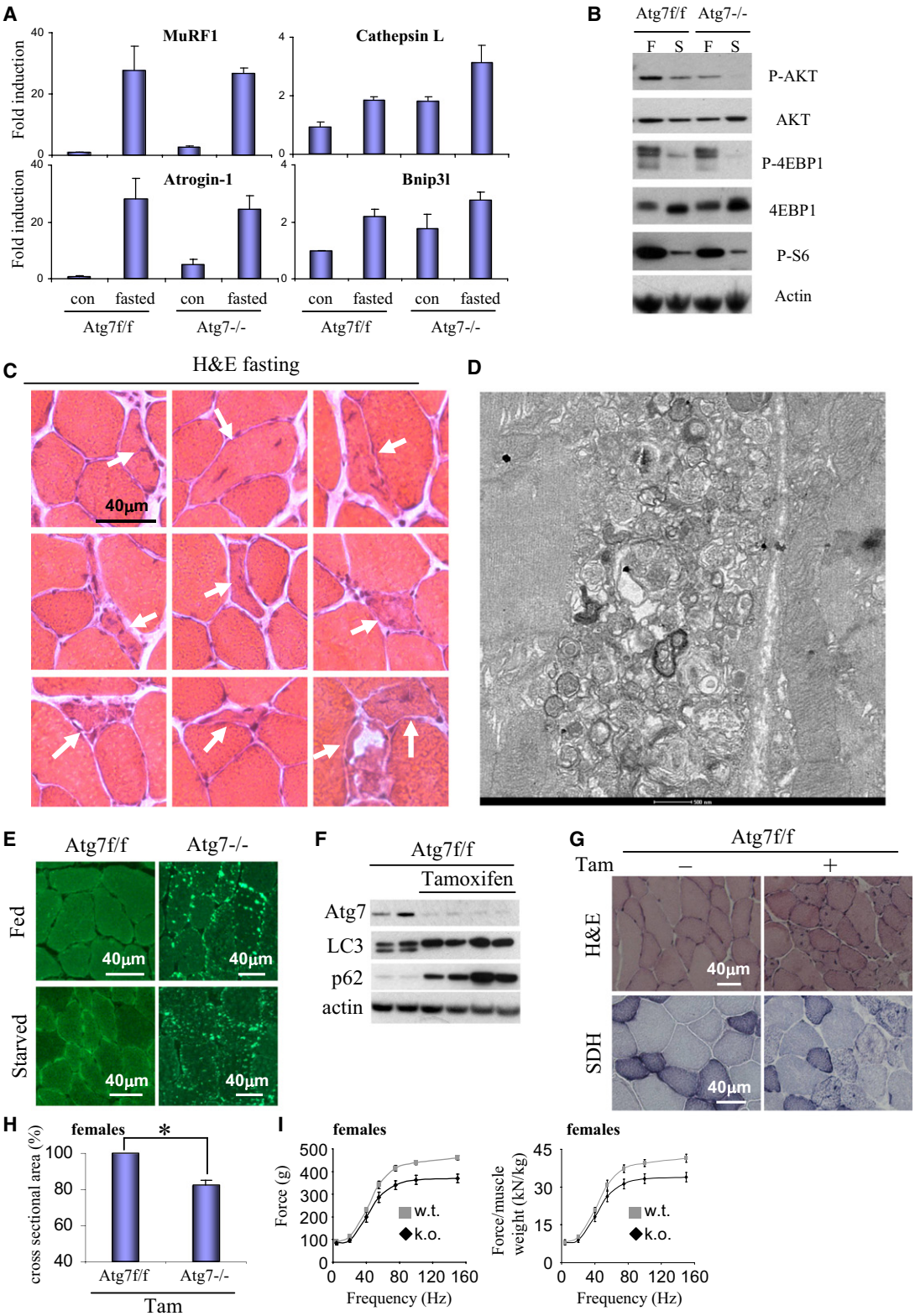

Figure 4. Atg7 Deficiency in Fasting and in a Tamoxifen-Inducible Muscle-Specific Atg7-Knockout Mice

(A) Upregulation of the atrophy-related genes in fasted skeletal muscles of Atg7$^{-/-}$ mice.

(B) Immunoblotting for insulin-dependent pathway in fed (F) and starved (S) muscles of Atg7$^{f/f}$ and Atg7$^{-/-}$ mice.

(C) H&E staining showing different features of muscle degeneration including small flattened or angulated atrophic fibers containing hematoxylin inclusion, central nuclei, vacuoles, and loss of plasma membrane integrity.

Immunoblotting analyses confirmed the *Atg7* deletion and the concomitant block of autophagy revealed by p62 accumulation and by inhibition of LC3 lipidation in glycolytic and oxidative muscles (Figures 4F and S1B). Morphological analyses showed the presence of structural alterations that are identical to those observed in non-inducible Atg7$^{-/-}$ muscle. Succinate dehydrogenase staining revealed accumulation of abnormal mitochondria in small atrophic fibers (Figure 4G). However, centrally nucleated fibers were more abundant after acute Atg7 deletion than in non-inducible autophagy-deficient muscles (Figure S5B). Indeed, when we measured muscle mass we found that autophagy inhibition triggered muscle wasting. Quantification of cross-sectional area showed a 20% decrease in myofiber size (Figure 4H), which was accompanied by a decrease in absolute and specific force (Figure 4I).

DISCUSSION

Our results indicate that basal autophagy plays a beneficial role in controlling muscle mass. Lack of autophagy affects the organelle shaping machinery and leads to accumulation of atypical giant mitochondria and dilated sarcoplasmic reticulum. However, accumulation of abnormal organelles is not always harmful for cellular function. In fact, ablation of *p62* in liver-specific autophagy-deficient mice suppresses pathological phenotypes including severe hepatomegaly, inflammation, and leakage of hepatic enzymes despite accumulation of abnormal organelles in the mice (Komatsu et al., 2007). Therefore, at least in autophagy-deficient liver, the presence of degenerated mitochondria might be hardly attributed to the phenotypes. Conversely, loss of p62 in neural-specific Atg7$^{-/-}$ mice does not suppress the pathology. Neurons from both single Atg7$^{-/-}$ and Atg7/p62 double knockout accumulate large number of abnormal organelles in the axon terminals, suggesting that an appropriate turnover of organelles in axon terminal is essential for neuronal homeostasis (Komatsu et al., 2007). Therefore, we can conclude that pathogenesis of cellular dysfunction and degeneration during autophagy inhibition differs among tissues and cell types.

In muscle, the persistence of dysfunctional organelle seems to be important for the activation of catabolic pathways, which results in muscle atrophy and weakness. In our model, alteration in sarcoplamic reticulum reflects an unfolding protein response that suppresses protein synthesis while mitochondrial damage generates oxidative stress and apoptosis. Also, the induction of Bnip3, which promotes mitochondrial fragmentation and mitophagy, in Atg7$^{-/-}$ muscles might contribute to caspase activation and apoptosis by affecting permeability transition pore opening. The control of mitochondrial function seems to be crucial for preventing a cascade of signals that lead to muscle atrophy (Sandri et al., 2006). The accumulation of aged and dysfunctional mitochondria and their potential negative role for cell survival has been recently underlined by different genetic evidences. For instance, it has been shown that dysfunctional mitochondria contribute to the pathogenesis of Ullirich and Bethlem dystrophies (Angelin et al., 2007; Irwin et al., 2003; Merlini et al., 2008). Similarly, erythroid cells lacking Bnip3l show persistence of mitochondria, due to a block of autophagy, which causes premature cell death and anemia (Sandoval et al., 2008). It is unclear whether our data of oxidative stress in Atg7$^{-/-}$ muscle is mainly caused by accumulation of dysfunctional mitochondria due to a defect in mitophagy, as recently described in autophagy-deficient cells (Tal et al., 2009), or whether it is secondary to p62 aggregates (Mathew et al., 2009). Moreover Atg7$^{-/-}$ muscles showed activation of ER chaperones, such as BiP, as well as the phosphorylation of eIF2α, suggesting an ongoing unfolded protein response. The failure of protein-folding quality control in Atg7$^{-/-}$ mice induces endoplasmic reticulum stress, which can generate ROS, and suppression of protein synthesis, which can contribute to muscle atrophy.

Recently muscle-specific Atg5$^{-/-}$ mice have been generated (Raben et al., 2008), and their phenotype is similar though not identical to that of Atg7$^{-/-}$ mice. Both knockouts show muscle loss, protein aggregates, and accumulation of abnormal membranous structures. The main difference between the two studies is related to the lack-of-force impairment reported in Atg5$^{-/-}$ animals. However, muscle force in Atg5$^{-/-}$ mice was evaluated by an indirect test, the wire-hang test, which can be affected by many variables including fatigue, whereas we performed a direct physiological analysis of force measurement on gastrocnemius muscles. In conclusion, our results suggest that in skeletal muscle defects in organelle removal generate a signaling cascade, which induces profound muscle loss and weakness. It has been shown that the efficiency of autophagic degradation declines during aging, leading to accumulation of intracellular waste products (Salminen and Kaarniranta, 2009). Our results suggest that impaired autophagy may contribute to aging sarcopenia. Thus, to combat sarcopenia, it is important to maintain autophagy flux to rejuvenate organelles and to prevent accumulation of dysfunctional mitochondria and ER membranes, as well as to block excessive protein breakdown.

EXPERIMENTAL PROCEDURES

Generation of Muscle-Specific Atg7$^{-/-}$ Mice and In Vivo Transfection Experiments

Generation of muscle-specific Atg7$^{-/-}$ mice is described in Supplemental Data. In vivo transfection experiments were performed by intramuscular injection of plasmid DNA in tibialis anterior (TA) muscle followed by electroporation

(D) Electron micrograph of fasted Atg7$^{-/-}$ muscles.
(E) Immunostaining for p62 showed positive aggregates in Atg7$^{-/-}$ muscles.
(F) Immunoblotting for Atg7, LC3, and p62 proteins on muscle extracts from inducible Atg7$^{-/-}$ mice. Two weeks after the last tamoxifen injection, skeletal muscles were collected and analyzed.
(G) H&E staining showing a general decrease in myofiber size and accumulation of hematoxylin positive inclusions. SDH staining on serial sections showed an accumulation of abnormal mitochondria.
(H) Quantification of CSA of myofibers. Values are mean ± SEM of data from five mice in each group, at least 1000 fibers for each muscles were measured (*$p < 0.001$).
(I) Force measurements performed in vivo, data are mean ± SEM ($n = 5$).

as described (Mammucari et al., 2007). Muscles were removed at 8 days after transfection and frozen in liquid nitrogen for subsequent analyses. Denervation was performed by cutting the sciatic nerve of left limb while right limb was used as control. Muscles were collected 3 days after denervation for gene-expression studies and 14 days after denervation for morphological analyses.

Gene-Expression Analyses

Total RNA was prepared from TA muscles using Promega SV Total RNA Isolation Kit. Complementary DNA generated with Invitrogen SuperScript III Reverse Transcriptase was analyzed by quantitative real-time RT-PCR using QIAGEN QuantiTect SYBR Green PCR Kit. All data were normalized to β-actin. The oligonucleotide primers used are shown in Table S1.

Immunoblotting

Frozen gastrocnemius muscles were powdered by pestle and mortar and lysed in a buffer containing 50 mM Tris pH 7.5, 150 mM NaCl, 10 mM $MgCl_2$, 0.5 mM DTT, 1 mM EDTA, 10% glycerol, 2% SDS, 1% Triton X-100, Roche Complete Protease Inhibitor Cocktail, 1 mM PMSF, 1 mM $NaVO_3$, 5 mM NaF and 3 mM β-glycerophosphate. The samples were immunoblotted as previously described (Sandri et al., 2004) and visualized with SuperSignal West Pico Chemiluminescent substrate (Pierce). Blots were stripped using Restore Western Blotting Stripping Buffer (Pierce) according to the manufacturer's instructions and reprobed if necessary. Detergent-soluble and -insoluble fractions were obtained according to (Hara et al., 2006). A list of antibodies is shown in Supplemental Data.

Histology, Fluorescence Microscopy, and Electron Microscopy

Cryosections of TA muscles transfected with YFP-LC3 were examined in a fluorescence microscope as described (Mizushima et al., 2004). Cryosections of TA were stained for H&E, for SDH, PAS, anti-ubiquitin, and anti-p62. CSA was performed on TA as described (Blaauw et al., 2008; Mammucari et al., 2007). For electron microscopy, we used conventional fixation-embedding procedures based on glutaraldehyde-osmium fixation and Epon embedding.

Measurements of Muscle Force In Vivo

Muscle force was measured in a living animal as previously described (Blaauw et al., 2008). Briefly gastrocnemius muscle contractile performance was measured in vivo in anaesthetized mice using a 305B muscle lever system (Aurora Scientific, Inc.). Contraction was elicited by electrical stimulation of the sciatic nerve. Force developed by plantar flexor muscles was calculated by dividing torque by the lever arm length (taken as 2.1 mm).

SUPPLEMENTAL DATA

The Supplemental Data include 20 figures, Supplemental Experimental Procedures, and Supplemental References and can be found with this article online at http://www.cell.com/cellmetabolism/supplemental/S1550-4131(09)00310-6.

ACKNOWLEDGMENTS

This work was supported by grants from Agenzia Spaziale Italiana (OSMA project) to M.S. and S.S., from Telethon (S04009), AFM (14135), the Italian Ministry of Education, University and Research (PRIN 2007) and Compagnia San Paolo to M.S., from the European Union (MYOAGE, contract: 223576 of FP7 to M.S. and S.S.), from the Japan Science and Technology Agency to M.K. Atg7 antibody was a generous gift of Dr. T. Ueno. We gratefully acknowledged S. Burden for the gift of MLC1f-Cre mice and the FP6 EXGENESIS Integrated Project to S.S.

Received: March 29, 2009
Revised: August 9, 2009
Accepted: October 6, 2009
Published: December 1, 2009

REFERENCES

Angelin, A., Tiepolo, T., Sabatelli, P., Grumati, P., Bergamin, N., Golfieri, C., Mattioli, E., Gualandi, F., Ferlini, A., Merlini, L., et al. (2007). Mitochondrial dysfunction in the pathogenesis of Ullrich congenital muscular dystrophy and prospective therapy with cyclosporins. Proc. Natl. Acad. Sci. USA *104*, 991–996.

Blaauw, B., Mammucari, C., Toniolo, L., Agatea, L., Abraham, R., Sandri, M., Reggiani, C., and Schiaffino, S. (2008). Akt activation prevents the force drop induced by eccentric contractions in dystrophin-deficient skeletal muscle. Hum. Mol. Genet. *17*, 3686–3696.

Dobrowolny, G., Aucello, M., Rizzuto, E., Beccafico, S., Mammucari, C., Bonconpagni, S., Belia, S., Wannenes, F., Nicoletti, C., Del Prete, Z., et al. (2008). Skeletal muscle is a primary target of SOD1G93A-mediated toxicity. Cell Metab. *8*, 425–436.

Hara, T., Nakamura, K., Matsui, M., Yamamoto, A., Nakahara, Y., Suzuki-Migishima, R., Yokoyama, M., Mishima, K., Saito, I., Okano, H., and Mizushima, N. (2006). Suppression of basal autophagy in neural cells causes neurodegenerative disease in mice. Nature *441*, 885–889.

Irwin, W.A., Bergamin, N., Sabatelli, P., Reggiani, C., Megighian, A., Merlini, L., Braghetta, P., Columbaro, M., Volpin, D., Bressan, G.M., et al. (2003). Mitochondrial dysfunction and apoptosis in myopathic mice with collagen VI deficiency. Nat. Genet. *35*, 367–371.

Komatsu, M., Waguri, S., Ueno, T., Iwata, J., Murata, S., Tanida, I., Ezaki, J., Mizushima, N., Ohsumi, Y., Uchiyama, Y., et al. (2005). Impairment of starvation-induced and constitutive autophagy in Atg7-deficient mice. J. Cell Biol. *169*, 425–434.

Komatsu, M., Waguri, S., Koike, M., Sou, Y.S., Ueno, T., Hara, T., Mizushima, N., Iwata, J., Ezaki, J., Murata, S., et al. (2007). Homeostatic levels of p62 control cytoplasmic inclusion body formation in autophagy-deficient mice. Cell *131*, 1149–1163.

Lecker, S.H., Jagoe, R.T., Gilbert, A., Gomes, M., Baracos, V., Bailey, J., Price, S.R., Mitch, W.E., and Goldberg, A.L. (2004). Multiple types of skeletal muscle atrophy involve a common program of changes in gene expression. FASEB J. *18*, 39–51.

Lecker, S.H., Goldberg, A.L., and Mitch, W.E. (2006). Protein degradation by the ubiquitin-proteasome pathway in normal and disease states. J. Am. Soc. Nephrol. *17*, 1807–1819.

Levine, B., and Kroemer, G. (2008). Autophagy in the pathogenesis of disease. Cell *132*, 27–42.

Mammucari, C., Milan, G., Romanello, V., Masiero, E., Rudolf, R., Del Piccolo, P., Burden, S.J., Di Lisi, R., Sandri, C., Zhao, J., et al. (2007). FoxO3 Controls Autophagy in Skeletal Muscle In Vivo. Cell Metab. *6*, 458–471.

Mathew, R., Karp, C.M., Beaudoin, B., Vuong, N., Chen, G., Chen, H.Y., Bray, K., Reddy, A., Bhanot, G., Gelinas, C., et al. (2009). Autophagy suppresses tumorigenesis through elimination of p62. Cell *137*, 1062–1075.

Merlini, L., Angelin, A., Tiepolo, T., Braghetta, P., Sabatelli, P., Zamparelli, A., Ferlini, A., Maraldi, N.M., Bonaldo, P., and Bernardi, P. (2008). Cyclosporin A corrects mitochondrial dysfunction and muscle apoptosis in patients with collagen VI myopathies. Proc. Natl. Acad. Sci. USA *105*, 5225–5229.

Mizushima, N., Yamamoto, A., Matsui, M., Yoshimori, T., and Ohsumi, Y. (2004). In vivo analysis of autophagy in response to nutrient starvation using transgenic mice expressing a fluorescent autophagosome marker. Mol. Biol. Cell *15*, 1101–1111.

Mizushima, N., Levine, B., Cuervo, A.M., and Klionsky, D.J. (2008). Autophagy fights disease through cellular self-digestion. Nature *451*, 1069–1075.

Nakai, A., Yamaguchi, O., Takeda, T., Higuchi, Y., Hikoso, S., Taniike, M., Omiya, S., Mizote, I., Matsumura, Y., Asahi, M., et al. (2007). The role of autophagy in cardiomyocytes in the basal state and in response to hemodynamic stress. Nat. Med. *13*, 619–624.

Raben, N., Hill, V., Shea, L., Takikita, S., Baum, R., Mizushima, N., Ralston, E., and Plotz, P. (2008). Suppression of autophagy in skeletal muscle uncovers the accumulation of ubiquitinated proteins and their potential role in muscle damage in Pompe disease. Hum. Mol. Genet. *17*, 3897–3908.

Salminen, A., and Kaarniranta, K. (2009). Regulation of the aging process by autophagy. Trends Mol. Med. *15*, 217–224.

Sandoval, H., Thiagarajan, P., Dasgupta, S.K., Schumacher, A., Prchal, J.T., Chen, M., and Wang, J. (2008). Essential role for Nix in autophagic maturation of erythroid cells. Nature *454*, 232–235.

Sandri, M. (2008). Signaling in muscle atrophy and hypertrophy. Physiology (Bethesda) *23*, 160–170.

Sandri, M., Sandri, C., Gilbert, A., Skurk, C., Calabria, E., Picard, A., Walsh, K., Schiaffino, S., Lecker, S.H., and Goldberg, A.L. (2004). Foxo transcription factors induce the atrophy-related ubiquitin ligase atrogin-1 and cause skeletal muscle atrophy. Cell *117*, 399–412.

Sandri, M., Lin, J., Handschin, C., Yang, W., Arany, Z.P., Lecker, S.H., Goldberg, A.L., and Spiegelman, B.M. (2006). PGC-1alpha protects skeletal muscle from atrophy by suppressing FoxO3 action and atrophy-specific gene transcription. Proc. Natl. Acad. Sci. USA *103*, 16260–16265.

Tal, M.C., Sasai, M., Lee, H.K., Yordy, B., Shadel, G.S., and Iwasaki, A. (2009). Absence of autophagy results in reactive oxygen species-dependent amplification of RLR signaling. Proc. Natl. Acad. Sci. USA *106*, 2770–2775.

Temiz, P., Weihl, C.C., and Pestronk, A. (2009). Inflammatory myopathies with mitochondrial pathology and protein aggregates. J. Neurol. Sci. *278*, 25–29.

Wang, X., Blagden, C., Fan, J., Nowak, S.J., Taniuchi, I., Littman, D.R., and Burden, S.J. (2005). Runx1 prevents wasting, myofibrillar disorganization, and autophagy of skeletal muscle. Genes Dev. *19*, 1715–1722.

Zhao, J., Brault, J.J., Schild, A., Cao, P., Sandri, M., Schiaffino, S., Lecker, S.H., and Goldberg, A.L. (2007). FoxO3 coordinately activates protein degradation by the autophagic/lysosomal and proteasomal pathways in atrophying muscle cells. Cell Metab. *6*, 472–483.